

Influence of TiC-Nanoparticles on the material properties of AlSi10Mg manufactured by Laser Powder Bed Fusion

V. Lubkowitz¹, T. Scherer^{2,3}, V. Schulze¹, F. Zanger¹

¹ wbk Institute of Production Science, Karlsruhe Institute of Technology (KIT), Kaiserstr. 12, 76131 Karlsruhe, Germany

² Institute of Nanotechnology (INT), Karlsruhe Institute of Technology (KIT), Hermann-von-Helmholtz-Platz 1, 76344 Eggenstein-Leopoldshafen, Germany

³ Karlsruhe Nano Micro Facility (KNMFi), Karlsruhe Institute of Technology (KIT), Hermann-von-Helmholtz-Platz 1, 76344 Eggenstein-Leopoldshafen, Germany

Abstract

Additive manufacturing enables the production of complex lightweight components. However, the poor use of atomized metal powders poses a challenge in terms of ensuring flowability and new high-strength aluminum alloys are still lacking. Some investigations show that the mechanical properties of AlSi10Mg can be improved by adding TiC nanoparticles. This study aims to determine if the influence of small amounts of TiC additions, which are normally used to improve the flowability of fine powders, is also sufficient to improve the mechanical properties. It was found that the addition of 0.46 wt% TiC-Nanoparticles with a size of 50 nm led to a homogeneous grain size distribution and an increase of 16 % in yield strength, but a 32 % decrease in elongation compared to pure AlSi10Mg. Further, a strong median grain size reduction from 5.08 to 2.74 μm could be observed by adding 0.96 wt% of TiC-Nanoparticles.

1. Introduction

New drive systems are only one way to reduce greenhouse gas emissions in the mobility sector. Equally important is the further reduction of vehicle weights. This applies in particular to the aerospace sector. For weight reduction, new manufacturing processes such as additive manufacturing are a chance because they allow the production of bionic structures made of metal. Of disadvantage is their high cost, partly caused by the raw powder materials. Regardless of the process, all methods for producing metallic components require spherical powder materials with good flowability to apply them layer by layer to a building platform. For the production of these powders, only gas atomization can be considered, which requires a total energy consumption of 2.7 MJ/kg and an inert gas compared to 1.4 MJ/kg for much cheaper water atomization [1]. The critical point is that only a maximum of 63% of the gas-atomized powder can be used for the additive processes since up to 25 % of fine particles < 15-20 μm (depending on the material) have to be removed by sieving procedures. The fine particles reduce the flowability of the powders drastically. The weight forces acting on the fine particles are smaller than the Van der Waals forces acting between the particles, which leads to the cohesion of the loose material and does not allow uniform layer recoating [2]. This considerably reduces the material and energy efficiency of the processes. By adding nanoparticles, a higher percentage of the atomized powder can be used, resulting in higher efficiency. The nanoparticles increase the distance between the particles, which reduces the acting adhesion forces between them and thus improves the flowability. Lüddecke et al. were able to demonstrate this by increasing the surface roughness of various metal powders by coating them with 100 nm particles, which improved the flowability [3]. Gärtner et al. were able

to increase the fine fraction (particles $< 20 \mu\text{m}$) of AlSi10Mg and 316L to 37% & 32% of the total powder feedstock, respectively, by coating the particles with nanoparticles, resulting in a flowable powder [4]. Fulchini et al. further investigated the required amount of nanoparticles added to improve flowability. They found an ideal particle surface coverage of 20% nanoparticles [5]. Gärtner et al. investigated this effect in more detail and found that the optimal surface area coverage is 25% [4].

In addition to a more material-efficient and thus more cost-effective process, the industry also demands high-strength materials. The focus is on new aluminum materials that are stronger than the frequently used alloy AlSi10Mg. In metal-cutting production group 7xxx alloys are frequently used for structural components. However, these alloys are currently difficult to process in powder bed-based selective laser melting (PBF-LB) due to their susceptibility to hot cracking during welding [6]. Therefore, new alloys have been developed as an alternative. One example are scandium-reinforced alloys, which can increase tensile strength by 20% over AlSi10Mg due to nano coherent Al₃Sc precipitates [7]. Further improvement in properties can be achieved by the addition of zirconium and/or manganese. Finely distributed precipitates are formed which allow the aluminum alloys to be heat treated without grain growth, reducing stresses without decreasing strength compared to non-heat treated samples [8,9]. However, problematic in these approaches is the use of the rare element scandium, which has been classified as a critical raw material in the European Union due to its difficult availability [10]. In addition, the elements mentioned are very expensive, which limits economic production.

Alternatively, the strength of the alloy AlSi10Mg, which has already been widely studied, could be increased by reducing the grain size. This requires the addition of nucleating agents. Several studies have already addressed this approach. Gao et al. found that TiC –nanoparticles act as nucleating agents due to the misfit of the lattice constant between TiC and Al. By adding 10 wt% TiC the average grain size could be reduced from 11 μm to 3 μm . This led to a significant increase in strength and elongation [11]. Fan et al. did not use a tumbler to prepare the aluminum-TiC composite powders but developed an electrostatic charging method to attach the nanoparticles directly to the AlSi10Mg surface. Again, the addition of 5 wt% of TiC reduced the grain size and achieved equiaxed alignment. Fine grain hardening resulted in an increase in yield strength from 254 MPa to 338 MPa with similar yield strength. A significant reduction in elongation was also observed. This was halved from 5.72 % to 2.97 % [12].

For crack-free production of EN AW7075 in the PBF-LB process, Ti micro and TiN nanoparticles were used as nucleating agents to suppress the formation of dendritic arms along which hot cracks normally grow. Li et al. showed that both particles decrease the grain size effectively. The Ti microparticles dissolve in the molten aluminum and increase the melt viscosity which reduces the agglomeration of the TiN nanoparticles. Therefore more of the 0.9 vol% TiN nanoparticles directly act as nuclear agents. The strong grain refinement and increased interfacial adhesion between Al and TiN due to the Ti addition made it possible to additively produce EN AW7075 specimens with similar strength and elongation properties as compared to the wrought material [13]. Wu et al. reported similar mechanical properties of EN AW7075 when only adding 2 wt% of TiN nanoparticles. Further, he showed that the aluminum particle coating reduced the laser reflectance so the applied laser energy has to be reduced [14].

A further positive effect of TiC nanoparticles was reported by Qu et al. who stabilized the keyhole form and keyhole movement velocity by increasing the melt pool viscosity by adding 4.4 vol% nanoparticles to EN AW6061. This expands the process window for pore-free part production [15].

Linking the two presented property improvements by nanoparticles seems reasonable. However, small amounts of particles of about 0.25 wt% are required for the improvement of flowability, and only high additions between 5 and 10 wt% were investigated in terms of improvement of mechanical properties. This work aims to analyze if low additions of TiC nanoparticles for flowability improvement are already sufficient to effectively increase the mechanical properties. For this purpose, different amounts of TiC nanoparticles were mixed with AlSi10Mg by a 3D tumbling mixer. First, for each powder mixture with a small DoE, it was checked whether an adjustment of the process parameters is necessary because the reflection of the blends changes and whether the pore-free process window expands. Second test specimens were built for the characterization of mechanical properties. At least the influence on the grain structure was analyzed and the tensile test properties were determined.

2. Materials and methods

The TiC nanoparticles with a size of 50 nm were supplied by IoLiTec Ionic Liquids Technologies GmbH (Heilbronn, Germany) and the AlSi10Mg powder by m4p material solutions GmbH (Magdeburg, Germany). The chemical composition of the aluminum powder used was determined by X-ray fluorescence (XRF) or optical emission spectrometry with inductively coupled plasma (ICP-OES) by the supplier, Table 1. The particle size distribution was determined dry by laser diffraction using a Cilas 1090, Figure 1 left. The powder shows usual distribution values of d_{10} : 35.82 / d_{50} : 52.9 / d_{90} : 74.95 μm . Due to the poor availability of fine aluminum powders, the influence of the fine content could not be considered. The approximately spherical morphology of the powder was determined by scanning electron microscopy (SEM), Figure 1 right.

Table 1: Chemical composition of the AlSi10Mg and B4C powder particles in wt%.

	Fe	Si	Mg	Mn	Ti	Zn	Cu	Pb	Sn	Ni	Al
AlSi10Mg	0.18	9.8	0.35	0.01	0.03	0.01	<0.01	<0.01	<0.01	<0.01	base

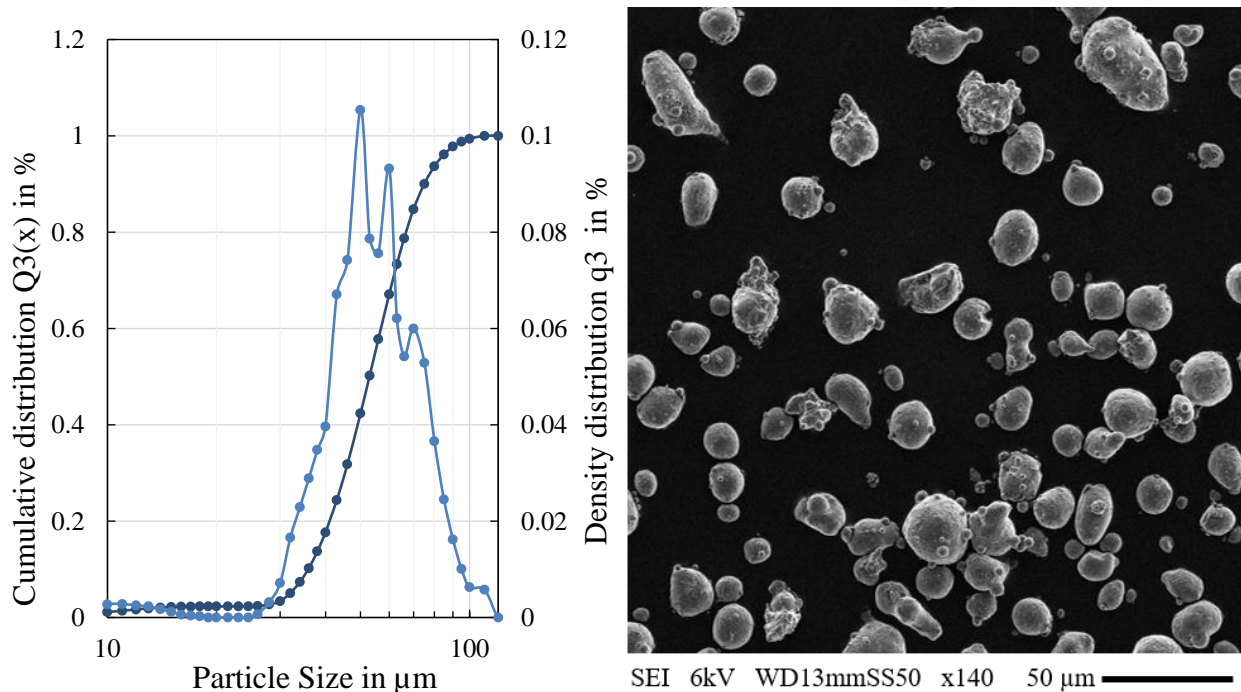


Figure 1: Particle size distribution (left) and SEM image of the AlSi10Mg powder (right)

Calculation of TiC nanoparticle addition

The necessary amount of TiC nanoparticles to cover a portion of the AlSi10Mg particle surface is calculated using a spherical model previously presented by Fulchini et al. [5]. For the calculation, it is assumed that all particles exist as an ideal sphere and have the same size, the cross-sectional area of the TiC nanoparticles covers the entire surface portion, are homogeneously distributed, and deposit as a single layer on the AlSi10Mg. The following formula 1 is obtained to calculate the TiC weight as a function of the AlSi10Mg weight to be covered and the desired surface area coverage:

$$w_{TiC} = \frac{16 \times w_{Al} \times (d_{TiC}/2)^3 \times \rho_{TiC}}{\rho_{Al} \times (d_{50,Al}/2) \times SAC \times d_{TiC}} \quad (1)$$

w_{TiC} : weight TiC

w_{Al} : weight AlSi10Mg

$d_{50,Al}$: mass median diameter of AlSi10Mg

ρ_{Al} : density of AlSi10Mg

d_{TiC} : mass median diameter of TiC

ρ_{TiC} : density of TiC

SAC : Surface area coverage

The calculated mass fractions of TiC considered in this study are shown in Table 2.

Table 2: Mass fraction of TiC for set surface area coverages

SAC in %	25	50	100
w_{TiC} in %	0.23	0.46	0.92

Coating process

The surface coating of the AlSi10Mg particles was carried out in a self-designed 3D tumble mixer, which has two separately controllable, perpendicularly aligned axes. The powder fractions were weighed with a PCB 3500-2 precision scale from Kern & Sohn GmbH and filled into a 2 l powder bottle from AMproved GmbH (Paderborn, Germany). The powders were then mixed for 30 min at a speed of 37 rpm on axis one and 47 rpm on axis 2. Every ten minutes, the direction of rotation of both axes was inverted. During the mixing process, collisions and friction between the particles occur, causing the nanoparticles to deposit on the aluminum particle surface and form satellites, which are held to the larger particles by Van der Waals forces. The TiC nanoparticles appear on SEM images as small white dots (only a few pixels in size) on the surface of the AlSi10Mg particles. With increasing SAC the number of attached particles increases. However, a 25/50/100 % occupation of the surface is not achieved, Figure 2.

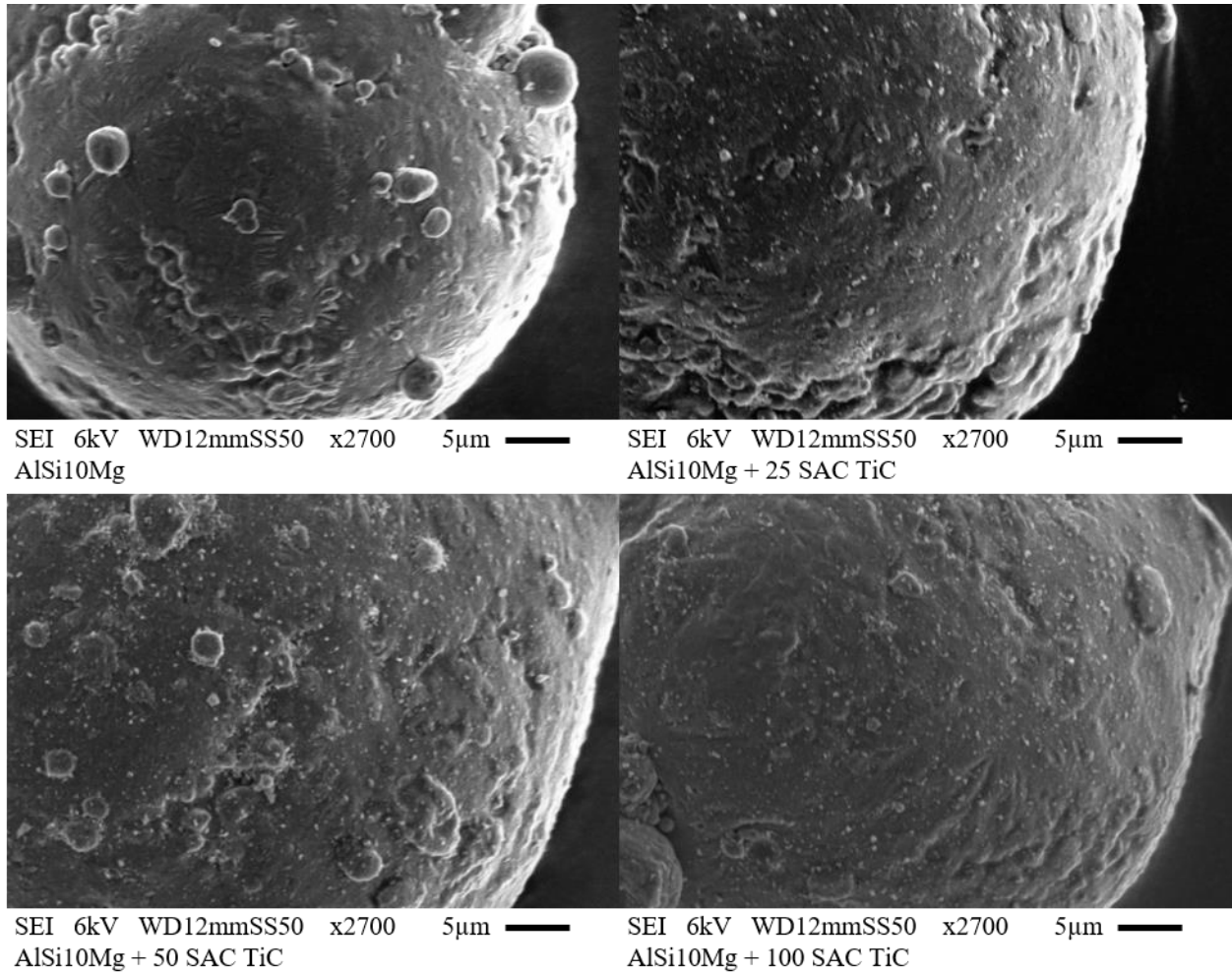


Figure 2: TiC-Nanoparticle coating on AlSi10Mg powder particles after mixing

Flowability of coated particle feedstocks

The Hausner-Ratio was determined to describe the powder flowability which is the ratio of tap and bulk density. The bulk density was measured according to ISO 3923-2 standard using a Scott Volumeter from 3P Instruments GmbH & Co. KG (Odelzhausen, Germany). The tap density was measured according to the ISO 3953 standard using a BeDensi tap machine from 3P Instruments GmbH & Co. KG (Odelzhausen, Germany). The overall scatter was calculated with the Gaussian scatter propagation.

The data show that the Hausner-Ratio decreases significantly with the addition of 25 SAC TiC, which means that the flowability increases significantly. The studied material behaves identically to the results of Fulchini et al. and confirms that the ideal improvement in flowability is achieved at a theoretical surface coverage of 25 SAC. At a surface coverage of ≥ 50 SAC, the nanoparticles not only increase the distance between the AlSi10Mg particles but also act as interlocking points and hinder the sliding of the particles against each other. For this reason, the flowability decreases again and is identical to the uncoated material at 100 SAC coverage, Figure 3. It can be deduced that the addition of nanoparticles should not exceed 50 SAC if both flowability and strength should be increased.

It should be highlighted that the absolute change in Hausner-Ratio is very small. This is because only already flowable material was investigated in this study. This also shows that the

Hausner-Ratio is suitable for detecting the smallest differences in the flowability of metal powder materials.

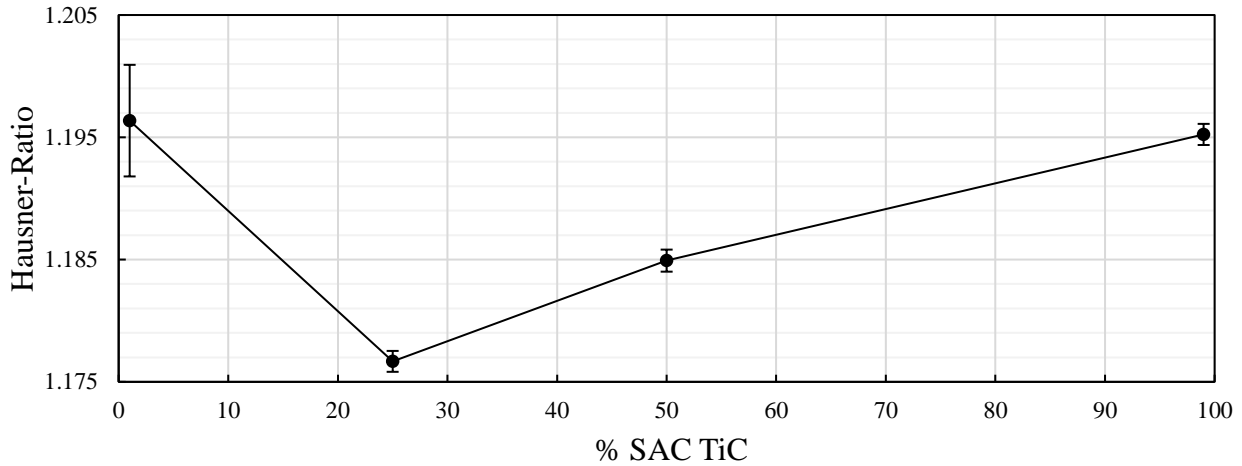


Figure 3: Influence of different surface area coverage values on the Hausner-Ratio of flowable AlSi10Mg

Production of test specimens in the PBF-LB process

A SLM280HL machine from SLM Solutions Group AG (Lübeck, Germany) was used for the manufacture of the specimens with a layer thickness of 50 μm and without platform preheating. The system is equipped with a 1070 nm ytterbium fiber laser from IPG. The laser beam is focused in the plane to w_0 : 81 μm with a Varioscans system. The beam has a Rayleigh length of z_R : 3.57 mm. To avoid oxidation effects, the build chamber is flooded with argon. The oxygen density was adjusted to below 200 ppm during the build job.

To keep the powder material consumption low, a self-developed build chamber reduction with $\varnothing 100$ mm was used in combination with a self-developed coater carriage. The coater carriage has a sliding mechanism for a defined powder deposit of 540 mm^3 per layer and has its own powder tank. The individual layers were applied with two pairs of metal brushes, which were arranged at a distance of 2 mm from each other. The single metal brush combs are spare parts of an Arcam EBM from GE Additive (Norwalk, United States of America).

Since a change in the laser energy degree of coupling and an increase of keyhole pore-free process window due to the powder coating was assumed, a small parameter study was first carried out to determine the process parameters with which the highest possible density can be achieved in the PBF-LB process. Only the line energy density ($\text{LED} = \text{laser power}/\text{scan velocity}$) was varied at a constant hatch distance of 0.17 mm. Three cylindrical specimens with a diameter of 11 mm were built for each LED setting. After the build-up, the specimens were cut flat at the top and then cut to a length of 10 mm from the build platform using wire EDM. Subsequently, the cylindrical outer surface was turned smooth to an average diameter of 10 mm. The actual dimensions of the specimens were then measured using an outside micrometer Micromar 40 ER from Mahr GmbH (Göttingen, Germany), and the weight was determined using an XSR204 precision scale from Mettler Toledo GmbH (Greifensee, Switzerland). The density of the specimens was then calculated. Archimedean density determination was excluded due to air bubble adhesion on the surface, especially on additively manufactured specimens, resulting in too large errors for small specimens.

The analysis of the test specimens shows a minimal increase in density with the addition of TiC, which is attributed to the higher density of the TiC particles. The expected shift of the highest

density to the lower LED could not be observed. It is assumed that the low amount of small nanoparticles is directly entrapped by the aluminum melt and thus cannot have any influence on the laser energy degree of coupling. This also confirms the results of Wu et al. who also did not adjust the process parameters up to an addition of 1 wt%. An adjustment was first necessary from 2 wt% [14]. Further, it can be seen that the ideal density for all specimens is achieved at an LED of 304 J/m. Deviations from the ideal LED decrease the density, especially at high LED and the process becomes unstable due to the increasing process pore formation as described in [16], Figure 4. Stabilization of the keyhole is therefore not reached with small additions of TiC nanoparticles as reported for huge amounts by Qu et al. [15].

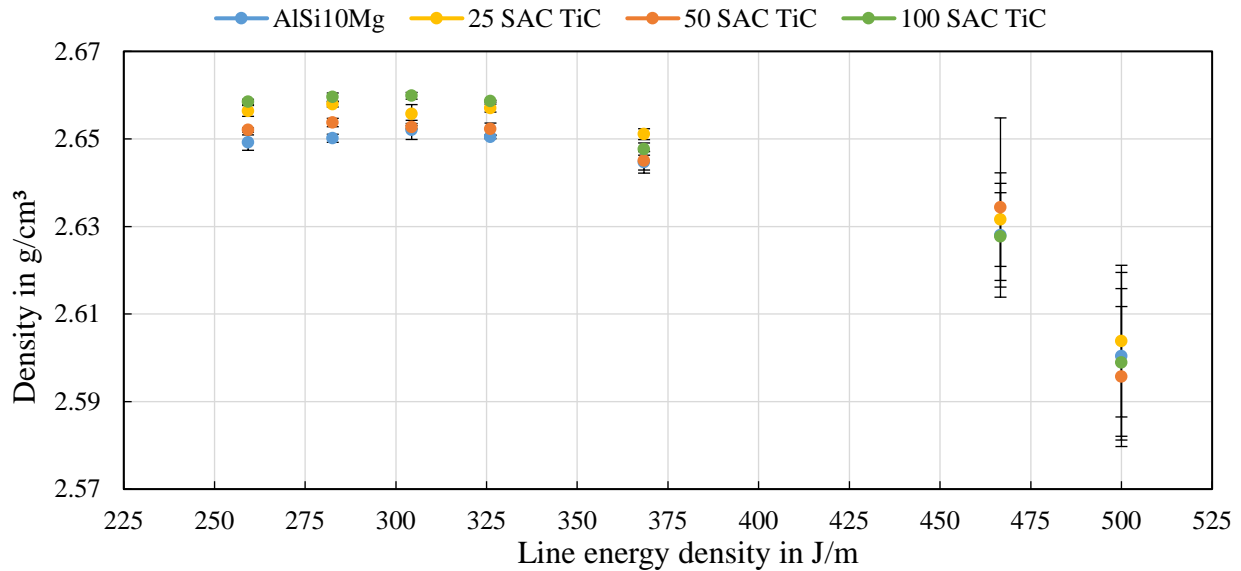


Figure 4: Change in density of cylindrical specimens as a function of line energy density for different surface area coverage values.

Measurement of mechanical properties in tensile test

Based on the density measurement results, cylinder specimens were additively fabricated from pure AlSi10Mg, 25 and 50 SAC powders using process parameter settings of laser power 350 W, scan velocity 1150 mm/s, and hatch spacing 0.17 mm. After the additive process, the test geometry was turned. To eliminate the effects of surface roughness and edge porosity, which occur during additive manufacturing, the surface layer was removed by turning, Figure 5.

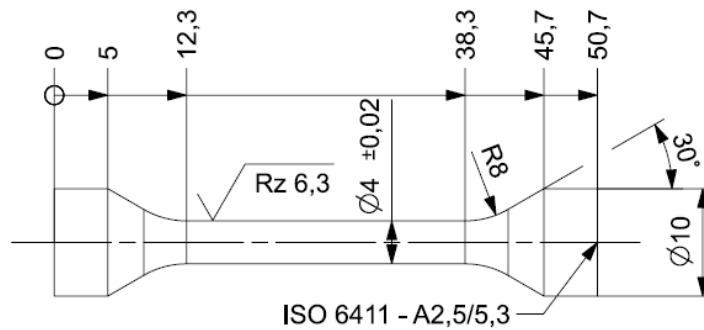


Figure 5: Design of tensile test specimen

The tensile test was carried out according to DIN EN ISO 6892-1 on a tension-compression testing machine from ZwickRoell GmbH & Co. KG equipped with a 200 kN load cell.

Electron backscatter diffraction (EBSD) for grain size and orientation analysis

Measurements were carried out using an Auriga 60 FIB-SEM from Carl Zeiss (Oberkochen, Germany) equipped with a Digiview EBSD camera from EDAX (Pleasanton, USA). For all measurements, the samples were embedded in Epoxy 2000 and mechanically high-grade polished using alkaline Silica suspensions with a grain size of 0.2 μm for the final polishing step from Cloeren Technology GmbH (Wegberg, Germany). The samples were carefully grounded with Cu foil to avoid any drift and prevent orientation artifacts. EBSD-orientation maps were recorded using 20 kV acceleration voltage with 120 μm aperture in high-current mode for 14 hours each. Data analysis was performed using EDAX OIM Analysis 8.6 software.

3. Results and Discussion

The orientation image map (OIM) of the EBSD measurements, Figure 6, for pure AlSi10Mg shows that fine grains form along the outer edge of a weld track and larger ones in the center of the weld track. This inhomogeneous grain size distribution is resolved by the addition of TiC nanoparticles. Up to an addition of 50 SAC TiC, the orientation of the grains in the direction of the build platform and/or in the direction of heat dissipation is maintained. When adding 100 SAC TiC, the grain structure changes again. A clear grain refinement can be seen and the grains have an equiaxed alignment.

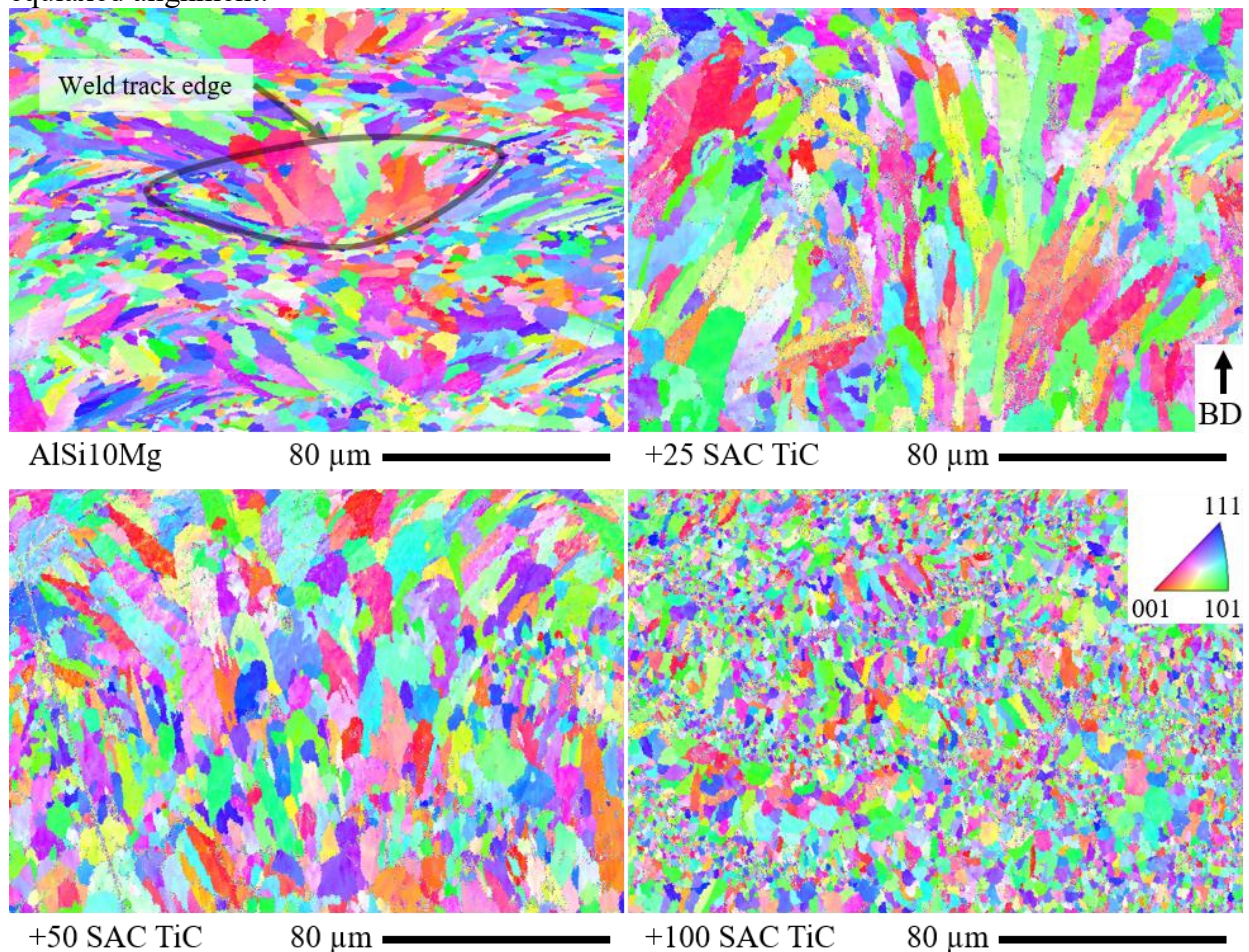


Figure 6: SEM-EBSD maps showing the different grain structures for different added amounts of TiC-nanoparticles

The evaluation of the grain size distribution verifies the visual impression of the OIM. The evaluation of the median and the 50 % quantile of all grains show similar values up to an addition of 50 SAC TiC. However, a difference can be seen in the maximum measured grain size. It can be seen that the largest grains are formed without TiC nanoparticles and that large grains are continuously reduced by the addition of TiC. At 100 SAC TiC, the median grain size is reduced to 2.74 μm and the grain size distribution becomes significantly smaller, Figure 7. From the observations, it can be deduced that not all TiC nanoparticles function as nucleating agents for a grain and a clear oversupply of nucleating agents is necessary to initiate effective grain refinement.

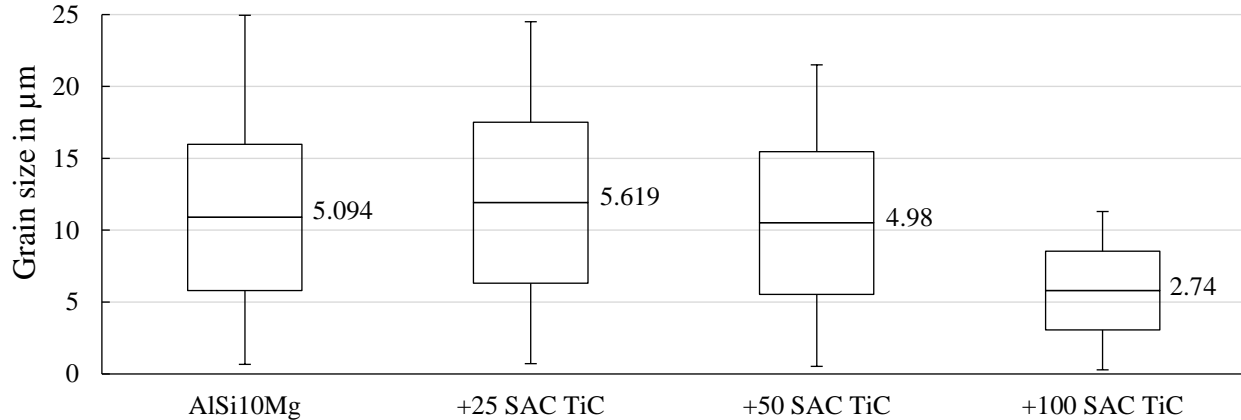


Figure 7: Grain size distribution depending on the added amount of TiC-nanoparticles

The tensile test analysis shows similar tensile strengths for all specimens. The yield strength, however, increases with the addition of TiC nanoparticles from 240 to 277 MPa with an addition of 50 SAC TiC. The elongation decreases continuously, Figure 8. The trends of the property change confirm the findings of Fan et al. [12]. However, the absolute measured elongation is significantly lower. This is attributed to the missing building platform heating. The associated higher cooling rate of the melt in the process leads to a stronger formation of the Si network around the submicron primary Al cells, which hinders the dislocation movement [17,18].

The increase in yield strength due to the addition of TiC compared to pure AlSi10Mg is not attributed to a change in the total grain size but to the inhomogeneous distribution inside the melt pool and at the melt pool edges. The large grains in the inner part of the melt pools hinder the dislocation movement less, causing the plastic deformation to start earlier.

Since the best flow-enhancing properties are achieved at 25 SAC, the DoE was initially planned only for 0, 25 and 50 SAC TiC. For this reason, only powder for density specimens was available. Even if the tensile tests are missing it is assumed that similar properties can be achieved with 100 SAC TiC as observed by Fan et al. as the measured grain refinement is similar. The addition of about 1 wt% thus appears to be the lower limit to significantly improve the mechanical properties. Even though the addition of 100 SAC TiC does not optimize the flowability of fine powders in the best way, a significant flowability improvement can still be achieved by this addition as Fulchini et al. and Gärtner et al. clearly show [4,5]. For this reason, more efficient use of atomized powder in the PBF-LB process is possible by adding small amounts of TiC nanoparticles and simultaneously improving the mechanical properties.

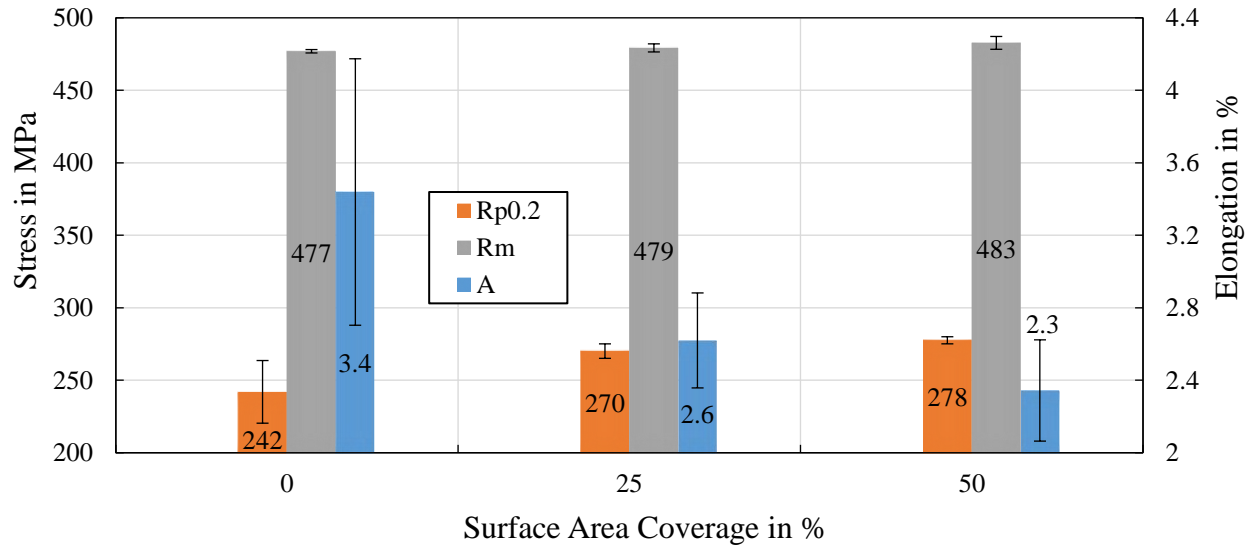


Figure 8: Properties of tensile test depending on the added amount of TiC-Nanoparticles

4. Conclusion and Outlook

In this work, the influence of small additions of TiC nanoparticles, which are normally used to improve the flowability of fine powders, on the grain structure and mechanical properties were determined. Three different additions of nanoparticles were investigated to cover 25, 50 and 100 % of the surface area of AlSi10Mg particles, respectively. This corresponds to 0.23, 0.46 and 0.96 wt%, respectively. The findings can be summarized as follows:

- To increase the flowability the surface coverage should not exceed 50 SAC.
- TiC nanoparticles on the AlSi10Mg particle surface do not change the coupling degree of the laser, so no adjustment of the process parameters is required due to the addition.
- The addition of TiC nanoparticles homogenizes the grain size distribution. There are no longer any differences between the weld track edge and the core as in the case of pure AlSi10Mg.
- The addition of 50 SAC TiC already enables a 16% increase in yield strength.
- The disadvantage of the TiC nanoparticle addition is the disproportionate decrease in elongation compared to the increase in strength.
- Only with the addition of 100 SAC TiC enough nucleating particles are in the powder to allow effective grain refinement. Therefore, a significant increase in strength and flowability is not possible.
- The addition of 100 SAC TiC equiaxes the grain alignment.

In further investigations, the actual strength increase with the addition of 100 SAC TiC still needs to be investigated. Further specimens in different orientations should be fabricated and tested. It is assumed that the anisotropic material behavior of AlSi10Mg changes to an isotropic material behavior due to the equiaxed orientation of the grains. Lastly, the influence of heat treatment should also be studied to increase the elongation again. It is conceivable that the TiC nanoparticles act similarly to scandium, zirconium, or manganese excretions in the aluminum, avoiding grain growth during heat treatment, and maintaining strength but relieving internal stresses.

5. Acknowledgements

This Project is supported by the Federal Ministry for Economic Affairs and Climate Action (BMWK) based on a decision by the German Bundestag.

The authors thank Mr. Vahid Tavakkoli (INT) for assistance with the EBSD measurements. This work was partly carried out with the support of the Karlsruhe Nano Micro Facility (KNMFi, www.knmf.kit.edu), a Helmholtz Research Infrastructure at Karlsruhe Institute of Technology (KIT, www.kit.edu).

References

- [1] Azevedo JMC, CabreraSerrenho A, Allwood JM (2018) Energy and material efficiency of steel powder metallurgy. *Powder Technology* 328(39):329–36.
- [2] Schulze D (2014) *Pulver und Schüttgüter: Fließeigenschaften und Handhabung*. 3rd ed. Springer Berlin / Heidelberg, Berlin, Heidelberg.
- [3] Lüddecke A, Pannitz O, Zetzener H, Sehr JT, Kwade A (2021) Powder properties and flowability measurements of tailored nanocomposites for powder bed fusion applications. *Materials & Design* 202(1–2):109536.
- [4] Gärtner E, Uhlenwinkel V (2022) Nanosized additives enhancing metal powder flowability in Additive Manufacturing applications. *AWT-Fachkonferenz, Werkstoffe – Prozesse – Wärmebehandlung*:12–20.
- [5] Fulchini F, Zafar U, Hare C, Ghadiri M, Tantawy H, Ahmadian H, Poletto M (2017) Relationship between surface area coverage of flow-aids and flowability of cohesive particles. *Powder Technology* 322:417–27.
- [6] Stopyra W, Gruber K, Smolina I, Kurzynowski T, Kuźnicka B (2020) Laser powder bed fusion of AA7075 alloy: Influence of process parameters on porosity and hot cracking. *Additive Manufacturing* 35:101270.
- [7] Ludwig I INCREASING RESOURCE EFFICIENCY OF AVIATION BY INNOVATIVE MATERIALS AND BIONIC DESIGN FOR METAL COMPONENTS MADE BY ADDITIVE MANUFACTURING.
- [8] Jia Q, Rometsch P, Cao S, Zhang K, Wu X (2019) Towards a high strength aluminium alloy development methodology for selective laser melting. *Materials & Design* 174:107775.
- [9] Spierings AB, Dawson K, Dumitraschkewitz P, Pogatscher S, Wegener K (2018) Microstructure characterization of SLM-processed Al-Mg-Sc-Zr alloy in the heat treated and HIPed condition. *Additive Manufacturing* 20(0):173–81.
- [10] Europäische Kommission (2020) MITTEILUNG DER KOMMISSION AN DAS EUROPÄISCHE PARLAMENT, DEN RAT, DEN EUROPÄISCHEN WIRTSCHAFTS- UND SOZIALAUSSCHUSS UND DEN AUSSCHUSS DER REGIONEN: Widerstandsfähigkeit der EU bei kritischen Rohstoffen: Einen Pfad hin zu größerer Sicherheit und Nachhaltigkeit abstecken.
- [11] Gao T, Zhang S, Liu G, Sun Q, Liu J, Sun Q, Sun J, Wang Z, Liu X, Wang X (2021) A high strength AlSi10Mg alloy fabricated by laser powder bed fusion with addition of Al Ti C B master alloy powders. *Materialia* 16(11):101103.
- [12] Fan Z, Yan X, Fu Z, Niu B, Chen J, Hu Y, Chang C, Yi J (2021) In situ formation of D022-Al3Ti during selective laser melting of nano-TiC/AlSi10Mg alloy prepared by electrostatic self-assembly. *Vacuum* 188:110179.
- [13] Li X, Li G, Zhang M-X, Zhu Q (2021) Novel approach to additively manufacture high-strength Al alloys by laser powder bed fusion through addition of hybrid grain refiners. *Additive Manufacturing* 48:102400.
- [14] Wu W, Gao C, Liu Z, Wong K, Xiao Z (2021) Laser powder bed fusion of crack-free TiN/Al7075 composites with enhanced mechanical properties. *Materials Letters* 282:128625.
- [15] Qu M, Guo Q, Escano LI, Clark SJ, Fezzaa K, Chen L (2022) Mitigating keyhole pore formation by nanoparticles during laser powder bed fusion additive manufacturing. *Additive Manufacturing Letters* 3:100068.
- [16] Lubkowitz V, Alber J, Zanger F (2021) PBF-LB Process-Induced Regular Cavities for Lightweight AlSi10Mg Structures. *Materials (Basel, Switzerland)* 14(21).
- [17] Casati R, Hamidi Nasab M, Coduri M, Tirelli V, Vedani M (2018) Effects of Platform Pre-Heating and Thermal-Treatment Strategies on Properties of AlSi10Mg Alloy Processed by Selective Laser Melting. *Metals* 8(11):954.
- [18] Lubkowitz V, Fischmann P, Schulze V, Zanger F (2022) Influence of initial powder layer thickness and focus deviation on the properties of hybrid manufactured parts by Laser Powder Bed Fusion. *Procedia CIRP* 111(1–3):87–91.